Optimization-through optical design-of a multi-wavelength fiber-based Raman-lidar system in the near field for vertical aerosol measurements in the troposphere

P. Kokkalis[1], G. Georgoussis[2], A. Papayannis[1], D. Hatzidimitriou[3], J. Porteneuve[4],

R. E. Mamouri[1], and G. Tsaknakis[1]

[1]National Technical University of Athens, Department of Physics, Zografou, Greece, panko@central.ntua.gr
[2]Raymetrics SA, Gkyka Nera, Athens, Greece, georgoussis@raymetrics.gr
[3]National and Kapodistrian University of Athens, Faculty of Physics, Department of Astronomy, Ilissia, Greece
[4]Service d'Aéronomie–IPSL, Verrières-le-Buisson, France, jacques.porteneuve@aerov.jussieu.fr

ABSTRACT

The laser remote sensing (lidar) technique of the atmosphere is a very efficient tool to monitor the aerosol optical and microphysical properties in the troposphere. In the frame of the EARLINET-ASOS project (2006-2011) a multi-wavelength (355-532-1064-387-607 nm) Raman lidar station has been operated since March 2006 in Athens (37°98' N, 23°77' E, 200 m above sea level-asl.), Greece, at the Campus of the National Technical University of Athens (NTUA).

To optimize the optical performance of our lidar system, as well as the quality of the aerosol measurements, mainly in the near-field (i.e. in the lower troposphere), several quality assurance (QA) tests have been adopted in the frame of the EARLINET-ASOS project. Through an optical design code, we were able to simulate the ray-tracing of the laser backscattered signals acquired at various wavelengths (in the present work mainly the 532 nm wavelength is presented). Simulating the light paths through the different parts of the lidar receiving optics (i.e. the receiving telescope, the transmitting optical fiber, the wavelength separation box with the dichroic beamsplitters, the collimating optics, the interference filters and the photodetectors (PMTs: photomultiplier tubes and APD: avalanche photodiode at 1064 nm)), we were able to discriminate the differences between the theoretical values of the full overlap distance with the real ones of our lidar system.

Starting from the current design of our lidar system, we were able to propose a solution, enabling us to decrease the distance of the full overlap (DFO) down to values of the order of 600-800 m, instead of the existing DFO values of 1200-1500 m, using a programming code based on the Zemax© optical design tool.

1. INTRODUCTION

Lidar systems, have been successfully used in remote sensing of the atmosphere, with applications either in local and global scale studies, concerning particulate matter (aerosol) and specific climate relevant molecular gases, such as ozone and water vapour [1-2].

The lidar geometric form factor O(r), referred sometimes as the overlapping function, describes the overlap function between the emitted laser beam and the receiving telescope field of view of a lidar system, as a function of the distance r from the lidar system [3]. More specifically, it represents the probability that the laser radiation from the target plane at range r, reaches the optical detector. Thus, O(r) is unity, only if full overlap between the emitted laser beam and the receiving telescope's field of view, including all the optical components of the receiving part, is achieved.

The theoretical optical analysis of our lidar system shows that the distance of the full overlap should be of the order of 600 m height. This would enable to fully detect the winter lower PBL height over Athens. However, this theoretical value was not achieved, so a ray tracing code had to be implemented in order to decrease the overlap distance of our lidar system.

The overlap factor, as presented in this work, is not dependent only on pure geometry of the receiving telescope, the distance between emitter-receiver, the laser beam shape/divergence and the optical fiber coupling with the detection box. We show that the overlap factor depends, as well, on the total geometrical path from the receiving telescope down to the optical detectors (APDs/PMTs), including all optical parts (i.e. dichroic beamsplitters, collimating lens, interference (IFF) or other optical filters). Therefore, all optical parts have to be taken into account in order to achieve the optimization of a lidar system.

2. THE NTUA RAMAN-LIDAR SYSTEM

The lidar system of the National Technical University of Athens was designed to perform continuous measurements of suspended aerosol particles in the planetary boundary layer (PBL) and the free troposphere [4].The system is based on the second and third harmonic frequency of a compact, pulsed Nd:YAG laser that emits pulses of 110 and 65 mJ output energy at 532 and 355 nm, respectively, with a 10-Hz repetition rate. The optical receiver is a reflecting concave parabolic mirror, which induces low aberrations in its focal plane with a diameter T=300 mm and a focal length f=600 mm, directly coupled through an optical fiber to the lidar signal detection box (Fig.1).

The main advantage of such geometry is the ability to design compact lidar systems that combine more than one telescope, each with a fiber optic output. Furthermore, it enables the physical separation of the signal detection box from the receiving telescope, which is

© Proceedings of the 8th International Symposium on Tropospheric Profiling, ISBN 978-90-6960-233-2
Delft, The Netherlands, October 2009. Editors, A. Apituley, H.W.J. Russchenberg, W.A.A. Monna

especially advantageous for scanning lidar systems. The optical fiber used is made from fused silica and has a core diameter of f_b=1.5 mm. The holder of the optical fiber is placed on or near the focal plane, 600 mm away from the primary mirror. The distance between the center of the emitted laser beam and the receiving telescope axis is d_0=300 mm for the 532 nm beam. The diameter of the initial laser beam is g_0=10 mm and the beam divergence is 0.5 mrad [5]. The field of view φ (FOV) of the receiving telescope is determined by the diameter of the fiber and is given by:

$$\varphi = \frac{\text{aperture's stop diameter}}{\text{receiver's focal length}} = 2.5 \text{ mrad} \qquad (1)$$

According to Jenness et al. [6], the optimum match of the fiber's numerical aperture ($N.A._f$) to the telescope f/# requires that:

$$f\,/\#_{tel} = 0.5[(\frac{1}{N.A._f})^2 - 1]^{\frac{1}{2}} \qquad (2)$$

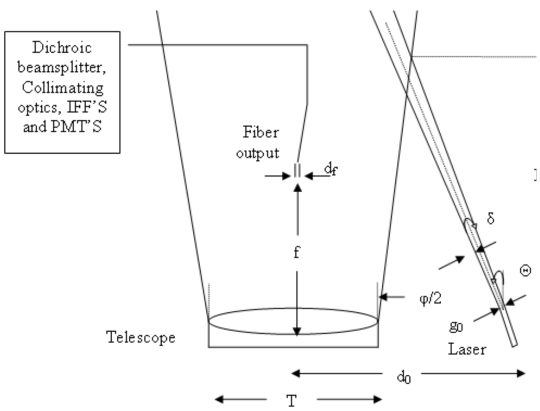

Figure 1. *The geometry of the telescope, laser and fiber's output system, of the NTUA's lidar system.*

In our case, since $N.A._f$ = 0.23, the ideal $f/\#_{tel}$ retrieved from Eq. (2) is 5.48% higher than the existing one, a fact which means that the existing fiber to telescope match is already close to its optimum value. Considering that the aperture stop of our lidar system is the fiber's core diameter, we determine the DFO according to Eq. 3 and Fig. 1, following the analytical description given by Stelmaszczyk et al. [7].

$$DFO = \frac{2d_0 + g_0 + T}{2\Theta + \varphi - \delta} \qquad (3)$$

From Fig. 2, it is obvious that the current lidar system should have approximately a DFO equal to 450 m (for 0 mrad inclination angle of the laser beam axis relative to the telescope axis). In addition, when the inclination increases, the DFO decreases, reaching a value of 180 m DFO for a 1.5 mrad inclination angle. However, these theroretical values of DFO were never found when using our lidar signals (Fig. 3.)

Small values of O(r) correspond to a situation in which a major part of the received laser beam is focused outside the detector's sensitivity area. For longer distances, the value of the O(r) increases, reaching unity, thus, the received laser beam is fully captured. For ranges r ≥ DFO, the laser beam stays entirely inside the telescopes' FOV. From Fig. 3, one can easily confirm that the expectable and the experimental values of DFO do not coincide.

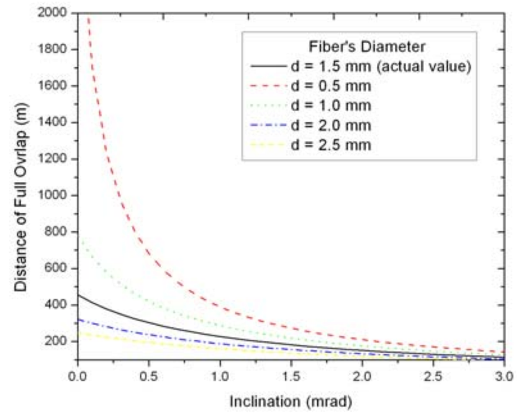

Figure 2. *The variability of DFO of NTUA's Raman lidar system as a function of the inclination angle and the optical fiber's diameter.*

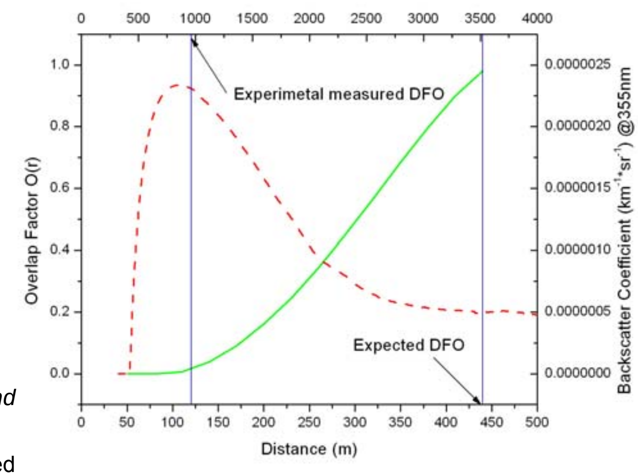

Figure 3. *The expected value of DFO according to the geometry of the telescope, laser and fiber's output system, and the experimental value of DFO calculated from measured lidar signals at 355 nm.*

3. SIMULATION OF THE SYSTEM THROUGH OPTICAL DESIGN

Many studies, of great success, have been performed concerning the simulation and the optimization of a lidar system using ray tracing codes [8]. Therefore, in order to investigate the reason of the difference found between the expected and the measured DFO values of our lidar system, a ray tracing simulation of our lidar system, including the telescope, the fiber, and all the optical components of the detection box, was performed through the Zemax© software [9]. In Fig. 4, we represent the spot diagram of the received light rays, that incident vertically on the fiber's core surface. It is obvious that both near (blue spots) and far field rays (green spots) are totally inside the fiber's core, something that could not explain the different DFO values (expected and measured).

Previous studies [8,10] have shown that apart the re-design of a lidar system with desirable specifications, the change of the laser beam inclination angle can give low DFO values. However, one should also consider, in advance, the position (and the relative distances) of the IFFs, the collimating lens, the detectors (PMTs/APD), and especially, the acceptance angle of the IFFS, in order to avoid third order aberration into the detection box. The acceptance angle of the IFF's, for our lidar system, should be lower than 1.5^0 for all wavelengths and specifically, 0.5^0 for the 532 nm channel.

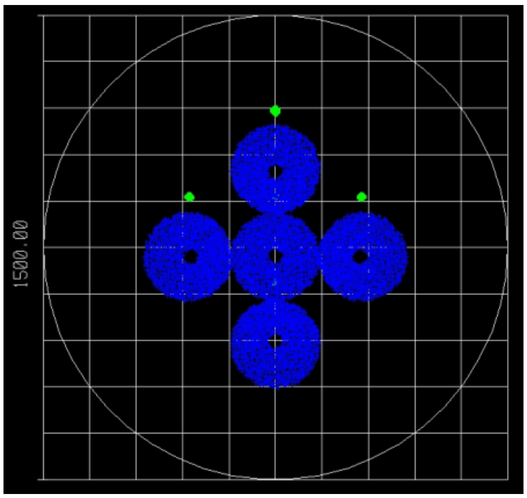

Figure 4. *The spot diagram, of near (blue) and far field (green) rays, that incident in the fiber's core surface.*

As an example, we give for the 532 nm channel, some useful geometrical specifications: DTI=312.4 mm, DTC=30.5 mm, f_c=33 mm and DCP=109.6 mm (DTI is the distance between telescope's focal point and the IFF, DTC is the distance between telescope's focal point and the collimating lens having focal length f_c and finally DCP is the distance between the collimating lens and the PMT.

From the ray tracing simulation of our lidar system, vignetting of the rays appears in the IFF, concerning the near field range (Fig. 5). The near field rays, specifically from 650 m range (Fig. 5, upper part), close to the expected value of the DFO~ 500 m, seem that all fall out of the IFF's surface. On the other hand, the rays coming from the far field (20 km range), seem to incident close to the middle of the IFF's surface, a fact that gives some tolerances to our optimization design. If the near field is set to 800 m (not shown), for the rays coming from that range, there is still some vignetting, although the bunch of rays is moving closer to the IFF's center. If the near field range is set to 1100 m (Fig. 5, lower part), the whole bunch of rays coming from that range, falls exactly at the IFF's surface. That range value is very close to the experimental value of DFO and is the value of the true DFO of our lidar system. Thus, we managed to confirm that due to the size of the IFF and the DTC the FOV was substantially decreasing in the near field, with consequences in the DFO value.

In order to reduce the true DFO value down to 650 m, we could decrease the distance between the collimating lens and the IFF. More specifically, increasing the DTC value, from 30.5 mm to 32 mm, we managed to decrease the DFO to our target value, but the acceptance angle of the IFF was increased up to 2^0, which overpasses the threshold value.

By tilting the laser beam from 0 to 0.5 mrad, we managed to solve the "vignetting" phenomenon concerning the 532 nm wavelength, but this did not work for the other channels (i.e. 387, 407 nm), since their ICL distances had even higher values.

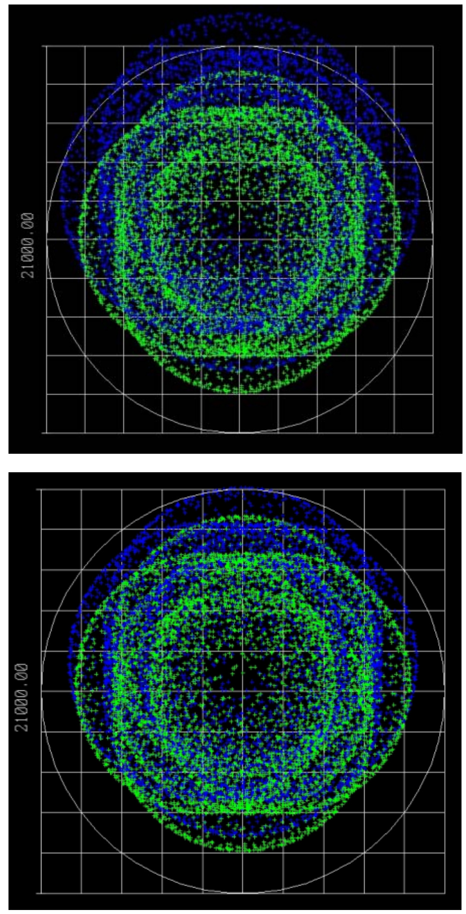

Figure 5. *The spot diagram, of near (blue) and far field (green) rays, that incident in the IFF's effective cross section surface. The upper one corresponds to near field set at 650 m range and far field set at 20 km range, while the second, to near and far fields set at 1100 m and 20 km, respectively.*

4. FINAL SOLUTION

Taking into account our previous results, we can propose two possible solutions. An affordable redesign of the lidar's detection box, through an extended ray tracing simulation, to obtain a more compact detection system with smaller distances between collimating lens-IFF and IFFs with bigger surface would, definitively, lead to a lidar system with no vignetting effects, but of very high cost. Since the building cost is of major importance, we propose the use of a beam expander (x3), in conjunction with a laser beam tilting up to 0.3 mrad. That solution fulfils all the conditions. No vignetting effects at any wavelength and acceptance angles lower than 1.5^0 for all the IFFs.

Supposing a lidar system with a laser beam expanded 3 times (laser beam divergence of ~0.17 mrad) and an inclination angle of 0.3 mrad, our simulation runs, for a near range of 650 m and a far range of 20 km, gave us the optimum solution, since no vignetting effects at any wavelengths were observed (shown here, in Fig. 6, for the 407 and 532 nm channels), for both near and far field rays. In this simulation the acceptance angle of the IFFs was smaller than the acceptable threshold value (1.5^0 for all wavelengths, except for the 532 nm channel where should be 0.5^0) .

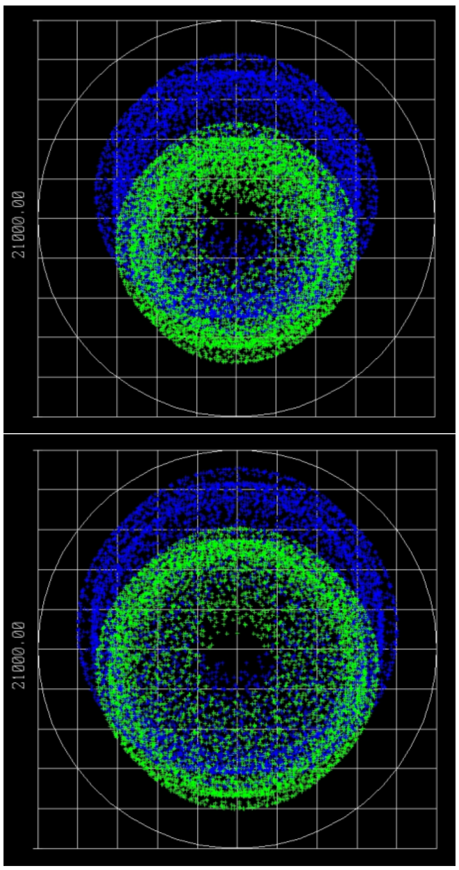

Figure 6. *The spot diagram, of near (blue, 650 m) and far field (green, 20 km) rays, that incident in the IFF's effective cross section surface. The upper one corresponds to the IFF's surface at 407 nm wavelength, while the lower one to the IFF's surface at 532 nm.*

In conclusion, to keep the cost minimum for the NTUA Raman lidar, the use of a laser beam expander (x3) in conjunction with a 0.3 mrad laser beam tilting, leads to a significant decrease of the DFO value down to 650 m, and therefore to an optimized lidar system. Both the near field and far field rays are then incident inside the IFF's effective surface, at all wavelengths.

ACKNOWLEDGEMENTS

Dr. Volker Freudenthaler is gratefully acknowledged for his technical comments and continuous help. The financial support for the improvement of the EARLINET infrastructure by the European Commission under grant RICA-025991 is gratefully acknowledged.

REFERENCES

[1] Papayannis, A., et al., 2008: Systematic lidar observations of Saharan dust over Europe in the frame of EARLINET (2000–2002), *Journal of Geophysical Research*, **113**, D10204, doi:10.1029/2007JD009028.

[2] Ansmann, A., M. Riedesell, U. Wandinger, C. Weitkamp, E. Voss, W. Lahmann, W. Michaelis, 1992: Combined Raman Elastic-Backscatter lidar for vertical profiling of moisture, aerosol extinction, backscatter, and lidar ratio*, Applied Physics,* **B55**, pp. 18-28.

[3] Kuze H., H. Kinjo, Y. Sakurada, N. Tackeuchi, 1998: Field-of-view dependence of lidar signals by use of Newtonian and Cassegrainian telescopes, *Applied Optics*, **37**, pp. 3128-3132.

[4] A. Papayannis, and G. Chourdakis, 2002: The EOLE Project: A multi-wavelength laser remote sening (lidar) system for ozone and aerosol measurements in the troposphere and the lower stratosphere. Part II: Aerosol measurements over Athens, Greece, *International Journal of Remote Sensing*, **23**, pp. 179-196.

[5] Chourdakis, G., A. Papayannis, and J. Porteneuve, 2002: Analysis of the receiver response for a non-coaxial lidar system with fiber-optic output, *Applied Optics*, **41**, pp. 2715-2723.

[6] Jenness, J. R., D. B. Lysak, and C. R. Philbrick, 1997: Design of a lidar receiver with fiber-optic output, *Applied Optics*, **36**, pp. 4278–4284.

[7] Stelmaszczyk, K., M. Dell' Aglio, S. Chudzyński, T. Stacewicz and L. Wöste, 2005: Analytical function for lidar geometrical compression form-factor calculations, *Applied Optics*, **44**, pp. 1323–1331.

[8] Freudenthaler, V., 2003: Optimized background suppression in near field lidar telescopes, 6th International Symposium on Tropospheric Profiling, Needs and Technologies.

[9] ZEMAX Development Corporation, San Diego, CA, USA, www.zemax.com

[10] Abramochkin, A. I., A.A. Tikhomirov, 1999: Optimization of a lidar receiving system. 2. Spatial filters, *Atmosphere and Ocean Optics*, **12**, pp. 331-342.